LES LONG-TERM ANALYSIS OF PARTICLES TRANSPORT IN MELT TURBULENT FLOW FOR INDUSTRIAL INDUCTION CHANNEL FURNACES

S.Pavlovs, *A.Jakovics* (Laboratory for Mathematical Modelling of Environmental and Technological Processes, Faculty of Physics and Mathematics, University of Latvia)

E.Baake, *B.Nacke* (Institute of Electrotechnology, Leibniz University of Hannover Germany)

INTRODUCTION

The *induction channel furnace* (ICF) is industrial metallurgical equipment with high electrical and thermal efficiency and is used for melting, holding and casting of metals and alloys, including cast iron and steel. Damages like erosion, clogging and infiltration of the ceramic lining in the channel as well as local overheating in the channel may lower the cleanness of the processed melt as well as the effectiveness and safety of ICF operation. The way to minimize these known problems is the choice of efficient regimes of melt circulation in ICF channel to provide controlled intensification of turbulent heat exchange between channel and throat.

As high temperature and flow velocity of the melt are extremely limiting the possibilities of experimental investigations of the heat and mass transfer and particle motion in ICF channel, the mathematical modelling based on *Large Eddy Simulation* (*LES*) approach is chosen for prediction of 3D transient temperature and velocity fields. The validity of *LES* approach has been verified by means of experimental and computational results' comparison obtained using experimental setups and ICF models [1]. Then verified *LES* approach has been applied for long-term computations of industrial ICF properties [2–5] including particles transport.

The *LES* study of particles' transport for industrial ICF has been performed using experience of cylindrical induction furnaces modelling [6,7]. The distributions of particle clouds and trajectories of separated particles are obtained along with *LES* modelled distributions of turbulent velocity and thermal fields using *Lagrangian* approach. The approach has been tested for ICF [6] and then applied further for a long-term computation of particle transport in the industrial ICF [3].

CONSIDERED MODELS OF INDUCTION CHANNEL FURNACE

The current paper presents the results of long-term computations of particle dynamics in the melt turbulent flow in industrial ICF with various designs of the channel. The set of considered ICF models consists of two different geometry designs with identical electrical induced power in the melt ($\approx 215kW$):

(1) The *model with two symmetric branches of the channel* (Figure 1, 2a) presents the original design of ICF, which has been previously introduced in [1]. The bottom part of ICF consists of channel, throat, inductor and iron yoke (Figure 2a), which are taken into account in EM modelling. Iron yoke is located around the right branch of channel at an angle $\alpha = -45^{\circ}$. The top part of ICF is a large cylindrical melt vessel or bath (Figure 1), which is taken into account only in HD and thermal modelling.

The origin of Cartesian coordinate system is placed at the geometrical centre of the ICF channel loop, where x-axis corresponds to the long side of the channel, y-axis – to the short, z-axis – to the vertical direction. The central angle α is counting clockwise as shown in the Figure 2 starting with an intersection of two perpendicular cross-sections $y = 0$ and $x = 0$.

(2) *Model with a considerably widened left branch of the channel* (Figure 2b) differs from the original design (Figure 2a) with gradual expansion of one branch from 100% cross-sectional area to 200% of cross-sectional area at the junction to the throat [1].

PECULIARITIES OF COMPUTATIONS

The numerical simulations are performed using commercial software packages *ANSYS* for EM field and *FLUENT* for HD, temperature fields and particle transport. The initial distributions of the melt velocity and temperature are obtained using steady state 3D standard k-ε model. For further computations the transient 3D *LES* model of turbulence is used.

The mesh for HD computations consists of approximately 3 million elements for symmetrical ICF and 6 million elements for asymmetrical ICF. The time step for transient HD computations is chosen as 0.005 sec. Computation time to obtain 1 sec of physical flow at *PC cluster* with 16 processor cores is 4–5 hours for a symmetrical ICF and 36–54 hours for an asymmetrical ICF. For post-processing of profile files prepared by *FLUENT* an own developed code is used [2].

LAGRANGIAN APPROACH FOR PARTICLE MOTION DESCRIPTION

According to *Lagrangian approach* disperse phase distribution is described as cloud of particles. Each particle of the cloud is described as a single point which moves with its own velocity.

The main assumptions regarding the particles' properties are the following:
- particles are rigid spheres;
- particles do not affect the structure and velocities of the melt flow;
- particle-particle interaction is negligible.

The motion of the each particle is determined by integrating the force balance in a *Lagrangian* reference frame

$$\frac{\mathrm{d}\mathbf{v}_p}{\mathrm{d}t} = \mathbf{f}_{drag} + \mathbf{f}_{buoyancy} + \mathbf{f}_{EM} \tag{1}$$

where v_p – particle velocity.

The forces acting to the particles, which are taken into account in equation (1), are drag, buoyancy and EM forces. The scheme of forces applied to light particle is shown in the Figure 3. The forces densities (i.e. force per unit of mass) are determined as follows.

√ ***Drag force*** acting to particle is appeared due to melt viscosity

$$\mathbf{f}_{drag} = \frac{18\eta_{melt}}{\rho_p d_p^2}\frac{C_D Re_\mathrm{p}}{24}\left(\mathbf{v}_{melt} - \mathbf{v}_p\right) \tag{2}$$

with drag coefficient for smooth spherical particle

$$C_D = \frac{24}{Re_\mathrm{p}}\left(1 + 0.15 Re_p^{0.687}\right) \tag{3}$$

and particle *Reynolds* number

$$Re_p = \frac{\rho_{melt} d_p \,|\,\Delta\mathbf{v}\,|}{\eta_{melt}} \tag{4}$$

where $\Delta\mathbf{v} = \mathbf{v}_{melt} - \mathbf{v}_p$ and ρ_{melt} and v_{melt} – melt density and velocity, ρ_p and d_p – particle density and diameter.

√ ***Buoyancy force*** acting to particle is appeared due to difference of particle and melt density

$$\mathbf{f}_{buoyancy} = \mathbf{g}\frac{\rho_{melt} - \rho_p}{\rho_p} \tag{5}$$

√ ***Electromagnetic force*** [8] acting to particle is appeared due to volumetric EM force in the melt

$$\mathbf{f}_p^{EM} = -\frac{3}{2}\frac{\sigma_{melt} - \sigma_p}{2\sigma_{melt} + \sigma_p}\mathbf{f}^{EM}V_p \tag{6}$$

where σ_p and V_p – particle electrical conductivity and volume, f^{EM} – EM force density in the point with particle coordinates, which is defined through application of the ICF model for EM computations.

For nonconductive particles $\sigma_p = 0$ the EM force acting on each particle is oppositely directed and has the maximal value

$$\mathbf{f}_p^{EM} = -\frac{3}{4}\mathbf{f}^{EM}V_p \tag{7}$$

Note that EM skin-layer thickness in the melt is corresponding (in order of magnitude) to characteristic radius of channel transversal cross-section but EM force acting on the particle is proportional to the third order of its diameter. The estimations, which have been performed in [9], show that for a small particle EM force is of the secondary significance in comparison with drag and buoyancy forces acting on the particle.

PROPERTIES OF PARTICLES FOR INDUCTION CHANNEL FURNACE SIMULATION

The particle transport simulations has been performed for ICF with symmetrical branches of channel (model (1)) and ICF with a widened left branch of channel (model (2)). The complete list of clouds' and separate particles' parameters is represented in the Table 1.

The main particles' features are the following:
• particles are chemically non-reactive with the melt;
• particles diameters are $d_p = 0.1$ mm;
• particles' density is $\rho_p \approx {}^3/_4\,\rho_{melt}$ except the case of the cloud in model (1) – $\rho_p \approx {}^1/_4\,\rho_{melt}$.

√ Particles *Reynolds* number (4), which is estimated separately for the channel and the bath (Table 1), is $Re_p \sim 40$–50 for ICF with different channel geometry regardless of different levels of maximal values of melt v_{melt} and particles' v_p, velocities in the channel and in the bath.

As $Re_p >> 1$ this fact means that the drag force is one of important factor for particles motion but particles cannot be interpreted as fluid tracers.

√ For *Stokes* number is defined as a ratio of the particle fluid response time constant to an appropriate turbulence time scale (dissipation time)

$$St = \frac{\rho_p d_p^2 v_{melt}}{18\eta_{melt} l_0} \tag{8}$$

where l_0 – characteristic length (see Table 1).

The estimations of *Stokes* number $St \sim 10^{-2}$–10^{-4} are also presented for different regions of the melt.

The *Stokes* number can be used for estimations of particles' movement character independently from other factors:
• if $St \ll 1$, then the particles' response to the fluid velocity changes is very fast;
• in an extreme case, when $St \to 0$, all the particles can be treated as the fluid tracers.

HOMOGENIZATION OF ALLOYING ADDITIONS AFTER THEIR INJECTION INTO THE MELT

The computations have been performed for model (1), flow time t = 10–555 sec (Figure 4). After t = 555 sec computation process for particle tracing has been interrupted due to the operative memory shortage for particles data storage in *FLUENT*.

A cloud of 16000 particles has been injected in the time point t = 10 sec in the region with its centre coordinates (0; 0.7; 1.6) as shown in the right sides of Figures 4a, 4b. Separated particles (totally 6) have been injected in the time point t = 10 sec in point with coordinates (0; 0.85; 1.6) as shown in the Figure 5b. Note, that the formulated conditions are only assumptions for estimation of melt *homogenization time*. The real sources of impurities are not discussed here.

The dynamics of particles' cloud long-term distribution in the bath is presented in the left side of Figure 4a, where relative integral number [%] of particles for horizontal layers with equal thicknesses is plotted as function of time flow. The choice of horizontal layers (from 1 to 10) in the bath is shown at right side of Figure 4a. For the throat and channel the particles' cloud distribution is presented in the left side of Figure 4b. The choice of horizontal layers in the throat and the channel (from 11 to 14 and from 15 to 22 accordingly) is shown at the right side of Figure 4b.

The most particles injected in the bath, which are lighter than the melt, remain in the bath – see example of separate particle's trajectory in Figure 5b. The distribution of particles' velocity in the bath is shown in Figure 5a. The characteristic velocity of particles in the bath is estimated as $v_p \sim 0.55$ m/s (Table 1).

As particles' velocities in the bath are for order of magnitude smaller in comparison with ones in the channel (Table 1) only the most "dexterous" particles reach the lower point of the channel or even return to the bath after travelling along the channel from the left outlet to the right [4, Figure 5e]. Thus numbers of particles for chosen layers in the throat are for order of magnitude smaller than in the bath as well as numbers of particles in layers in the channel is for order of magnitude smaller than in the throat – compare Figures 4a and 4b.

In the bath after particles' injection at flow time t = 10 sec the approximately uniform alloying additions' distribution for all chosen layers (except upper layer 1) is reached at flow time after t ≈ 130 sec (left side of Figure 4a). Thus the estimated ***time of homogenization*** of alloying additions is the following

$$t_{homogen} \sim 120 \text{ sec} \qquad (9)$$

The particles' number in upper layer 1 after $t_{homogen}$ is approximately two times greater than in the rest layers. This fact for analysed cases is the indication, that buoyancy force is more significant than the drag force for particles, which are lighter then the melt – $\rho_p \approx {}^3/_4 \rho_{melt}$.

DISTRIBUTION OF DISJOINTED IMPURITIES
DUE TO EROSION OF CHANNEL CERAMIC LINING

The computations have been performed for model (2) for flow time t = 95–200 sec (Figure 7) for cloud of 25000 particles and separated particles (totally 9). These particles are considered as impurities, which have been disjoined due to erosion of channel ceramic lining at time point t = 95 sec in channel's lower point with coordinates (0;0;-0.285) as shown in the right sides of Figure 7 and in Figure 8b. Note, that the formulated conditions are only assumptions for estimation of melt *contamination rate*. The real sources of impurities are not discussed here.

The dynamics of particles' cloud migration from the channel to the bath may be considered using in Figure 6, where integral number of cloud particles in the channel (totally and separately for left and right branches), in the throat and in the bath is shown as function of flow time, as well as in Figure 7, where relative integral number [%] of particles for horizontal layers with equal thicknesses is plotted as function of time flow. The choice of horizontal layers in the channel and in the throat (from 1 to 8 and from 9 to 12 accordingly) is shown in right side of Figure 7a. The choice of horizontal layers (from 13 to 2) in the bath is shown in right side of Figure 7b.

Cloud particles' velocities $v_p \sim 3$ m/s are very high only in the channel (Figure 8a) and corresponds to melt velocities v_{melt} in considered cross-sections of the channel [3]. That is why despite of the very small melt transit velocity $v_{melt}^{transit} \sim 4$ cm/s [3] the most "dexterous" particles may leave the channel for a very short time – in a few seconds after peeling off – see the example of separated particle track in [4, Figure 4e].

As direction of melt transit velocity $v_{melt}^{transit}$ is from the right branch to the left one of the channel, the integral number of particles in the left branch is greater than in the right branch (Figure 6). This fact may be illustrated by comparison of trajectory length in left and right branches of the channel for characteristic separate particle (Figure 8b).

To leave the channel and to reach the throat (left sides of Figures 6, 7a) for the first particles of cloud disjoined in the lower point of the channel, it is necessary only ~5 s (flow time t = 100 sec). After ~25 s (flow time t = 120 sec) ~40% of particles may be found in the bath (left sides of Figures 6, 7b). Travelling to the bath of ~80% particles have taken ~50 s (flow time t = 145 sec), but after ~ 70 s (flow time t ~ 165 sec) more than 90% of particles are in the bath (Figure 6).

These results make it possible to define and than estimate (see Figure 6) the ***contamination rate*** as the ratio of particles number N_{bath}, which have reached the bath, and total particles number N_{total}, per unit of time flow (for example t = 1 min):

$$\frac{N_{bath}}{N_{total}} \sim 85\% \qquad (10)$$

CONCLUSIONS

The following qualitative estimations have been obtained for considered cases of particle distributions:
√ estimated alloying additions' *homogenization time* in the melt bath is ~ 2 min after their injection;
√ peeled off impurities travel very rapidly from the channel to the bath;
√ the *contamination rate* of the melt in the bath (that is defined as relative number of particle travelled from the channel to the bath in 1 min of flow time) is ~ 85%;

√ buoyancy force significance is determinative for light particles' distribution near melt free surface in the bath.

Performed long-term computations have shown the effectiveness of *LES* approach application for predictions of particle transport along with transient characteristics of turbulent heat and mass exchange in industrial ICF. The validity of *LES* approach application for HD and thermal fields' modelling in ICF have been successfully verified by the comparison of experimental and computational results. However, there is a difficulty concerning the complex experimental verification of computational models of particles' transport in the high temperature non-transparent electrically conductive melts. This problem awaits the solution in the nearest future.

ACKNOWLEDGEMENTS

The current research was performed with the financial support of the ESF project of the University of Latvia, contract No. 2009/0223/1DP/1.1.1.2.0/09/APIA/VIAA/008.

REFERENCES

1. BAAKE E., JAKOVICS A., PAVLOVS S., KIRPO M. Influence of channel design on heat and mass exchange of induction channel furnace // COMPEL (The International Journal for Computation and Mathematics in Electrical and Electronic Engineering), 2011, Vol. 30, No. 5, pp. 1637–1650.
2. BAAKE E., JAKOVICS A., PAVLOVS S., KIRPO M. Numerical Analysis of Turbulent Flow and Temperature Field in Induction Channel Furnace with Various Channel Design // International Scientific Colloquium "Modelling for Material Processing", Riga, September 16–17, 2010, pp. 253–258.
3. BAAKE E., JAKOVICS A., PAVLOVS S., KIRPO M. Long-term computations of turbulent flow and temperature field in the induction channel furnace with various channel design // Magnetohydrodynamics, 2010, Vol. 46, Nr. 4, pp. 317–330.
4. JAKOVICS A., PAVLOVS S., KIRPO M., BAAKE E. Long-term LES Study of Turbulent Heat and Mass Exchange in Induction Channel Furnaces with Various Channel Design // Fundamental and Applied MHD, Borgo, Corsica, France, 2011, vol. 1, pp. 283–288.
5. PAVLOVS S., JAKOVICS A., BAAKE E., NACKE B., KIRPO M. LES modelling of turbulent flow, heat exchange and particles transport in industrial induction channel furnaces // Magnetohydrodynamics, 2011, Vol. 47, Nr. 4, pp. 399–412.
6. KIRPO M., JAKOVICS A., BAAKE E., NACKE B. LES study of particle transport in turbulent recirculated liquid metal flows // Magnetohydrodynamics, 2006, Vol. 42, No. 2, pp. 199–208.
7. KIRPO M., JAKOVICS A., NACKE B., BAAKE E. Particle transport in recirculated liquid metal flows. COMPEL: The International Journal for Computation and Mathematics in Electrical and Electronic Engineering, 2008, Vol. 27, No. 2, pp. 377–386.
8. LEENOV D., KOLIN A. Theory of electromagnetophoresis. I. Magnetohydrodynamic forces experienced by spherical and symmetrical oriented cylindrical particles // The Journal of Chemical Physics, 1954, Vol. 22, pp. 683–688.
9. SHCHEPANSKIS M., JAKOVICS A., BAAKE E. The statistical analysis of the influence of forces on particles in EM driven recirculated turbulent flows // Journal of Physics: Conference Series, 2011, Vol. 333, p. 012015.

Figure 1. ICF with symmetrical channel

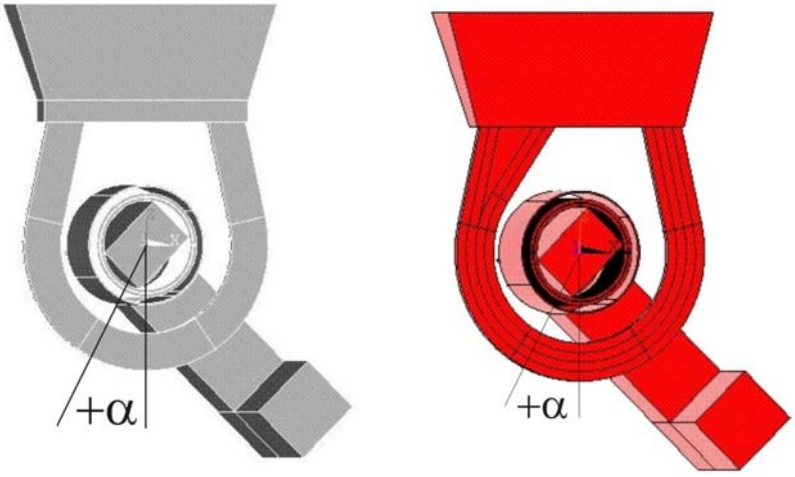

a *b*

Figure 2. ICF geometry for EM modelling:
(a) ICF with symmetrical channel;
(b) ICF with left widened branch of channel

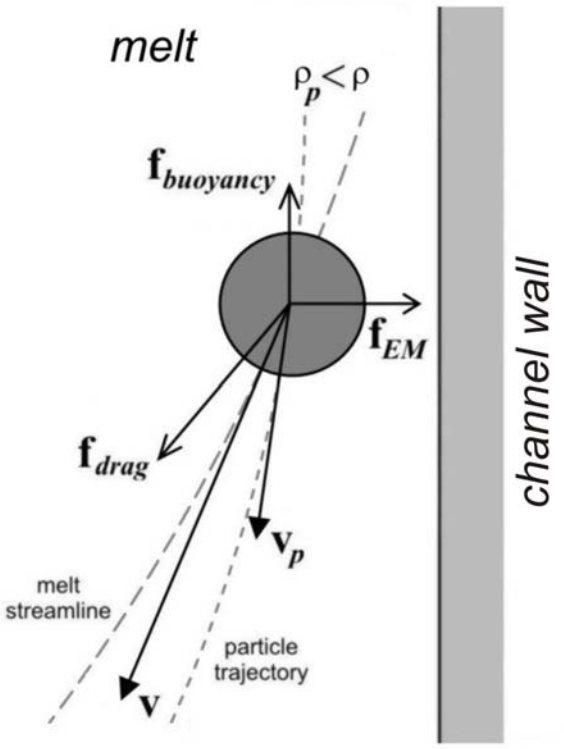

Figure 3. Schemes of forces acting to light particle ($\rho_p < \rho$) near channel wall of ICF

Table 1. Physical properties of particles clouds and separated particles

Parameter	**Symbol or formula**	**Unit**	**ICF channel geometry**			
			symmetrical – model (1)		***widened left branch – model (2)***	
			Particles clouds	Separated particles	Particles clouds	Separated particles
Obtained flow time	t	s	10–555		95–200	
Particles' electrical conductivity	σ_p	$(\Omega \cdot m)^{-1}$	0		0	
Particles' diameter	d_p	mm	0.1		0.1	
Characteristic length						
• smaller radius of channel cross-section	l_0	m	0.0599		0.0599	
• radius of bath			0.88		0.99	
Characteristic (maximum) instantaneous velocity for flow time point						
flow time point	t	s	555		200	
• particle in channel	v_p	m/s	1.08		2.04	
• particle in bath			0.055		0.085	
• melt in channel	v_{melt}		1.48		2.43	
• melt in bath			0.39		0.53	
Particle Reynolds number						
• in channel	$Re_p = \frac{\rho_{melt} d_p \lvert \vec{v}_p - \vec{v}_{melt} \rvert}{\eta_{mekt}}$		48.7		47.4	
• in bath			40.8		54.1	
Coordinates of particles injection center (cloud) or point	(x,y,z)	m	(0;0.7;1.6)	(0;0.85;1.6)	(0;0;-0.285)	(0;0;-0.285)
Particle density	ρ_p	$10^3 \cdot kg/m^3$	5.25	5.25	1.55	5.25
Particle and melt densities relationship	ρ_p/ρ_{melt}	%	77.1%	77.1%	22.8%	77.1%
Number of particles	N	–	16000	6	25000	9
Stokes number						
• in channel	$St = \frac{\rho_p d_p^2 v_{melt}}{18 \eta_{melt} l_0}$		$8.6 \cdot 10^{-4}$	$8.6 \cdot 10^{-4}$	$6.2 \cdot 10^{-3}$	$2.1 \cdot 10^{-2}$
• in bath			$2.3 \cdot 10^{-4}$	$2.3 \cdot 10^{-4}$	$8.1 \cdot 10^{-5}$	$2.4 \cdot 10^{-4}$

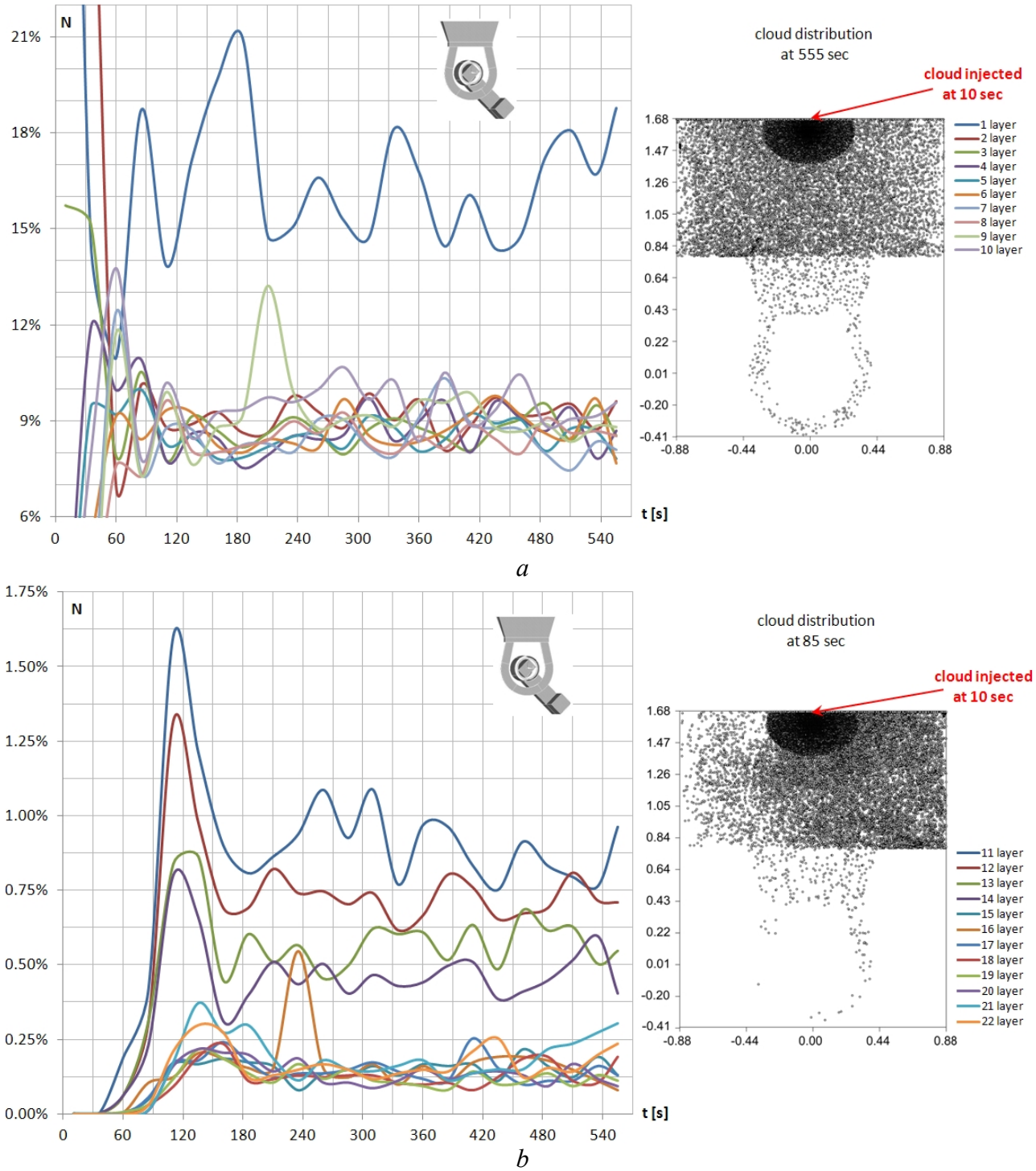

Figure 4. ICF with symmetrical channel, flow time 10–555 sec.
Relative numbers of 16000 particles ($\rho_p \approx {}^1/_4\,\rho_{melt}$) cloud for horizontal layers of equal thickness: 1–10 layers (a, right) for bath (a, left); 11–22 layers (b, right) for channel and throat (b, left). Distribution of particles cloud for flow time: t=555 sec (a, right), t=85 sec (b, right).

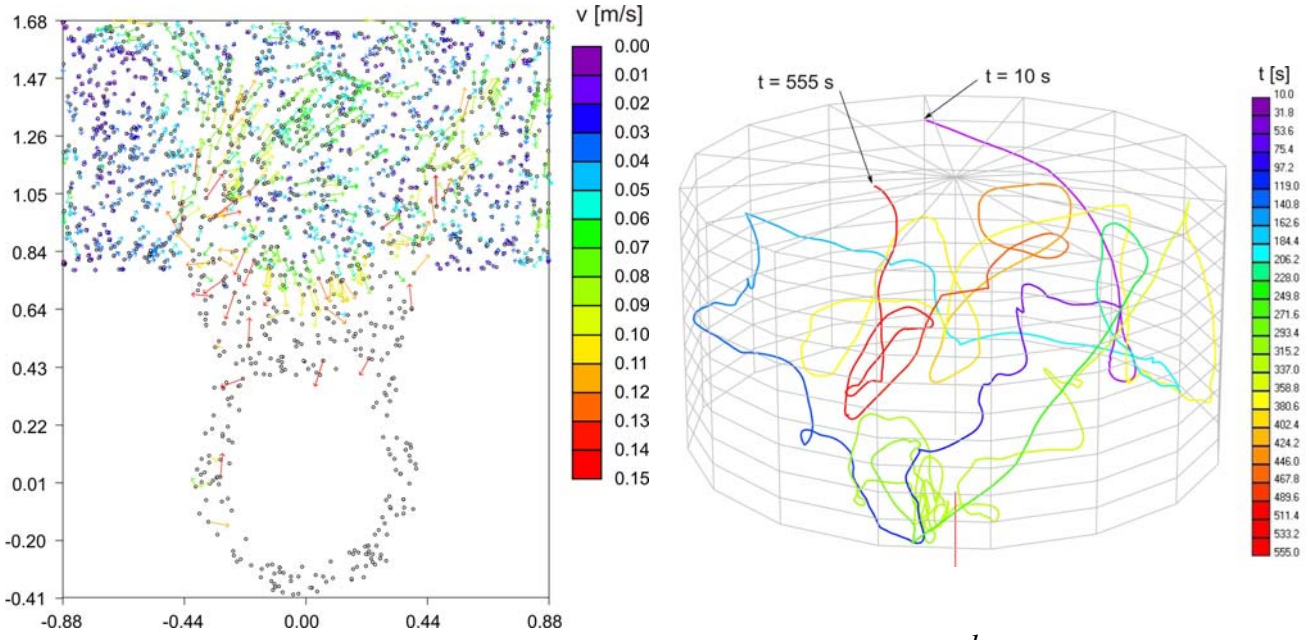

a *b*

Figure 5. ICF with symmetrical channel.
Cloud particles' ($\rho_p \approx {}^1/_4\,\rho_{melt}$) velocity vectors (only for $v_p < 0.15$ m/s !)
in the channel and in the throat (a) for flow time t=555 sec.
Track coloured by time (b) of single particle ($\rho_p \approx {}^3/_4\,\rho_{melt}$) for flow time t=10–555 sec.

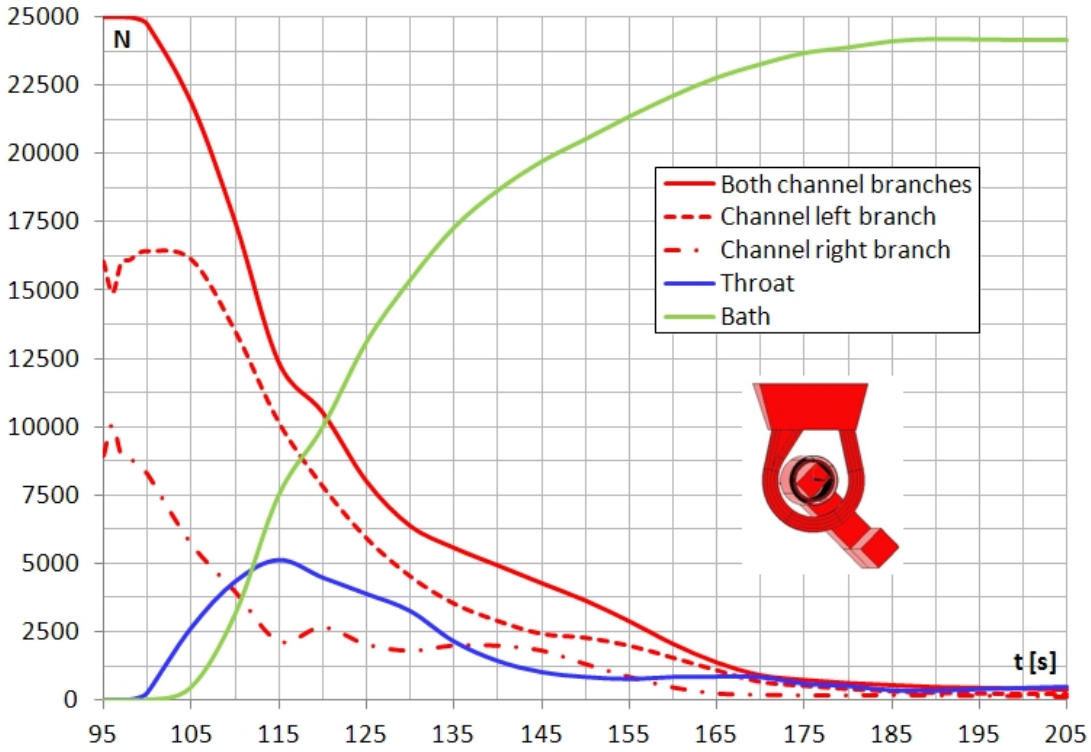

Figure 6. ICF with widened channel, flow time 95–200 sec.
Integral number of particles ($\rho_p \approx {}^3/_4\,\rho_{melt}$) in the channel, in the throat and in the bath.

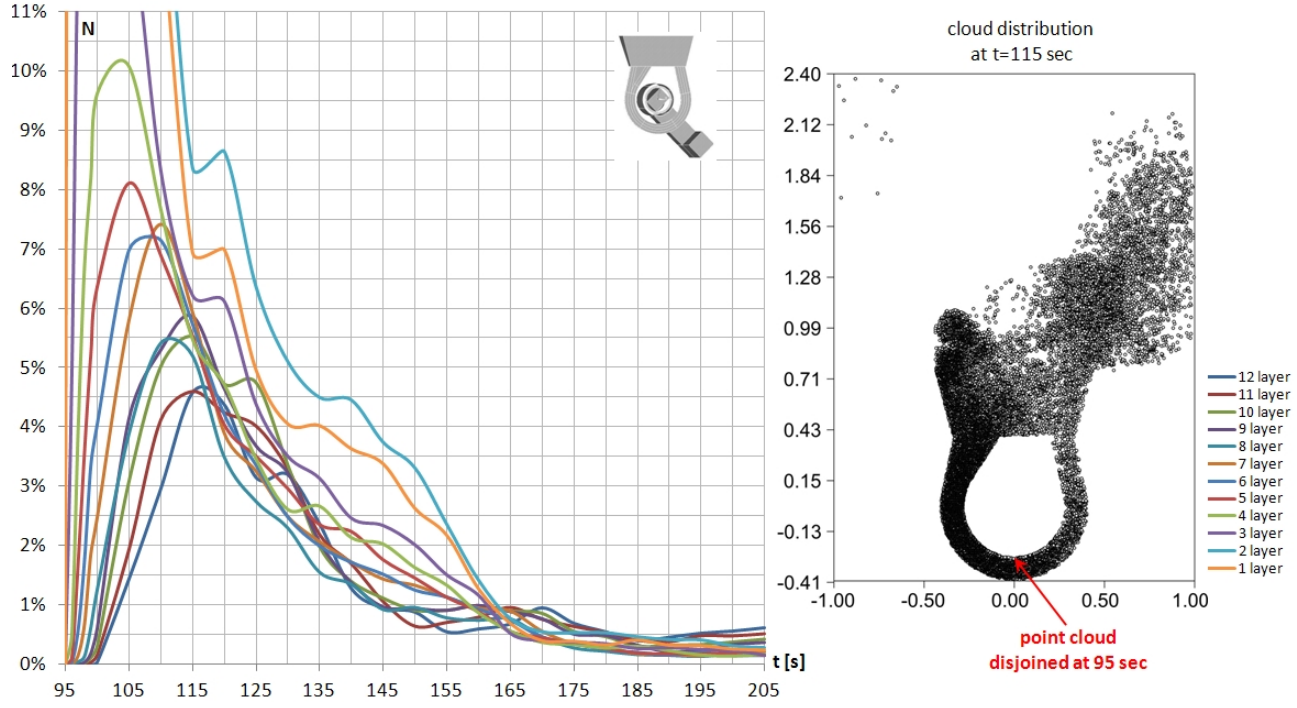

a

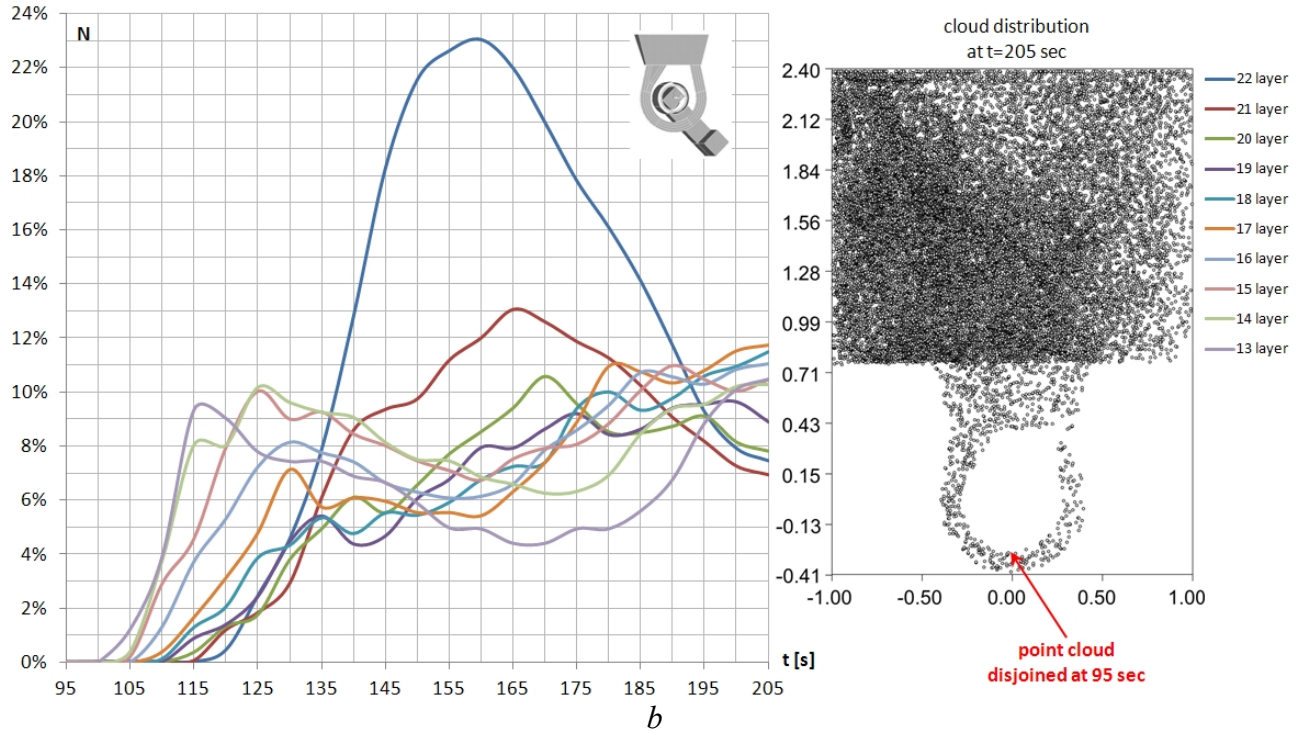

b

Figure 7. ICF with widened channel, flow time 95–200 sec.
Relative numbers of 25000 particles ($\rho_p \approx {}^3/_4\, \rho_{melt}$) cloud for horizontal layers of equal thickness: 1–12 layers (a, right) for channel and throat (a, left); 13–22 layers (b, right) for bath (b, left). Distribution of particles cloud for flow time: t=115 sec (a, right), t=205 sec (b, right).

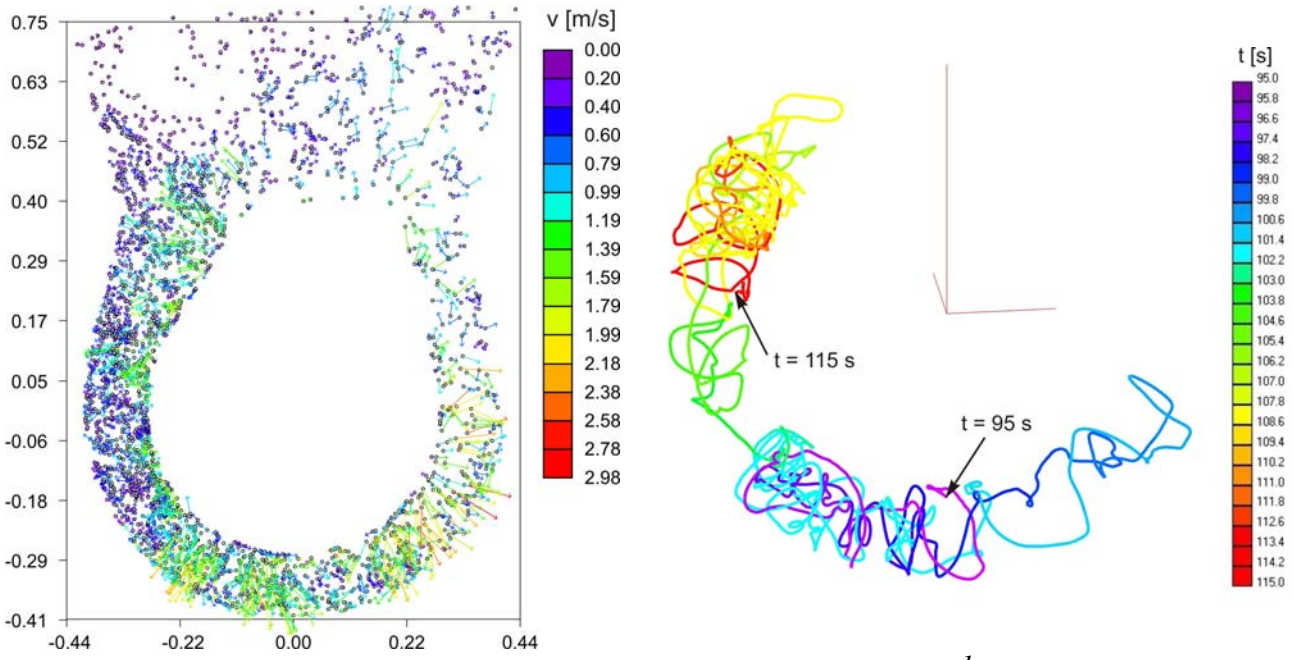

a *b*

Figure 8. ICF with widened channel.
Cloud particles' ($\rho_p \approx {}^3/_4\,\rho_{melt}$) velocity vectors in the channel and in the throat (a) for flow time t=125 sec.
Track coloured by time (b) of single particle ($\rho_p \approx {}^3/_4\,\rho_{melt}$) for flow time t=95–115 sec.